Electronic Supplementary Information

Non-isothermal kinetics of spin crossover

Mark B. Bushuev, *[a,b] Elena B. Nikolaenkova[c] and Viktor P. Krivopalov[c]

[a] Nikolaev Institute of Inorganic Chemistry, Siberian Branch of Russian Academy of Sciences, 3, Acad. Lavrentiev Ave., Novosibirsk, 630090, Russia, E-mail: bushuev@niic.nsc.ru, mark.bushuev@gmail.com; Fax: +7 383 330 94 89; Tel: +7 383 316 51 43.

[b] Novosibirsk State University, 2, Pirogova str., Novosibirsk, 630090, Russia.

[c] N. N. Vorozhtsov Novosibirsk Institute of Organic Chemistry, Siberian Branch of Russian Academy of Sciences, 9, Acad. Lavrentiev Ave., Novosibirsk, 630090, Russia.

Table of contents

Sample 14-1

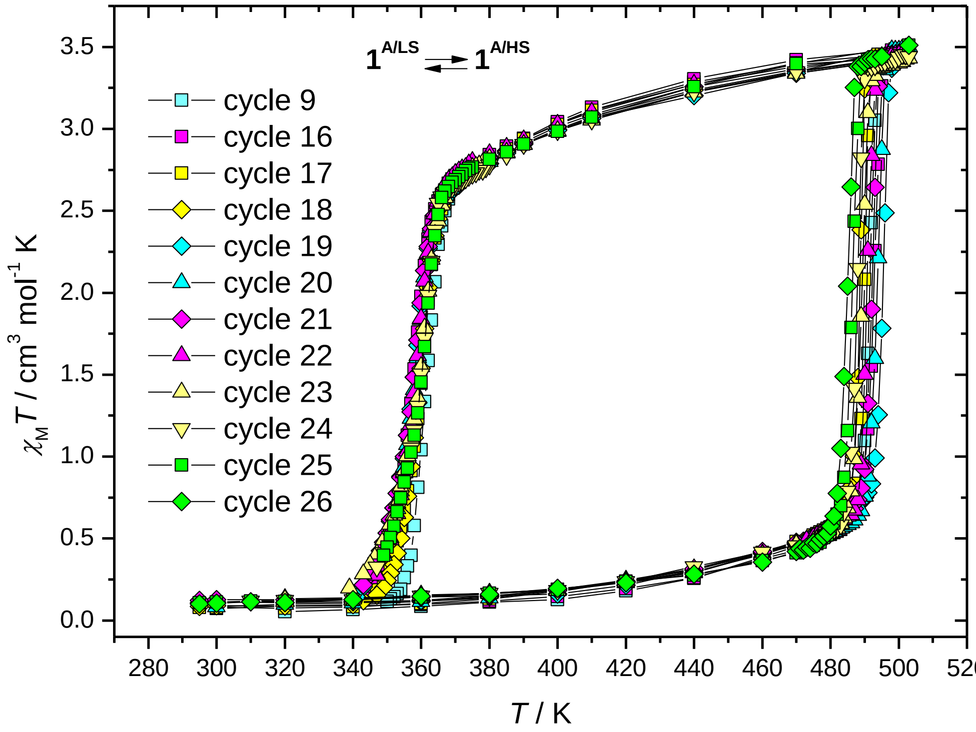

Fig. S1 Typical thermal cycles $\mathbf{1}^{A/LS} \leftrightarrow \mathbf{1}^{A/HS}$ for the sample **14-1**. Scan rates: 1 K min^{-1} (cycles 9, 19 and 20 cyan), 0.5 K min^{-1} (cycles 16, 21 and 22, magenta), 0.25 K min^{-1} (cycles 17, 18, 23 and 24, yellow), 0.1 K min^{-1} (cycles 25 and 26, green). At 460 K (cycle 15, the heating branch) no variation of the magnetic moment was observed for *ca*. 9 h (M. B. Bushuev, D. P. Pishchur, V. A. Logvinenko, Y. V. Gatilov, I. V. Korolkov, I. K. Shundrina, E. B. Nikolaenkova and V. P. Krivopalov, *Dalton Trans*., 2016, **45**, 107–120.).

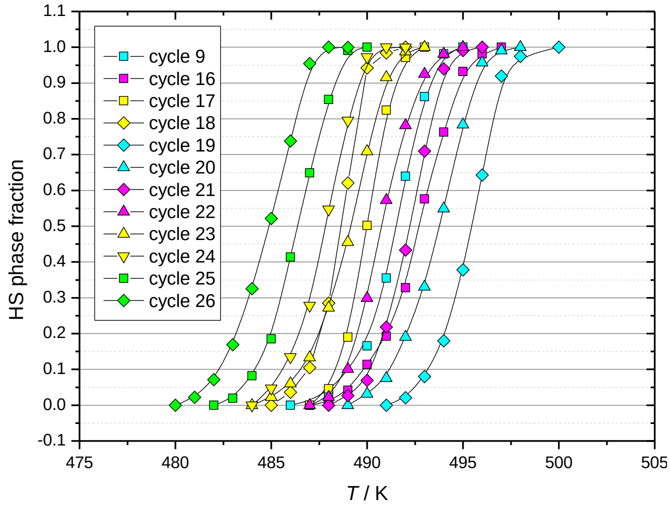

Fig. S2 The normalized heating branches of the $\chi_M T$ vs. T curves for the sample **14-1** (the procedure A was applied to extract the heating branches from the $\chi_M T$ vs. T curves). The solid lines are the B-splines.[1]

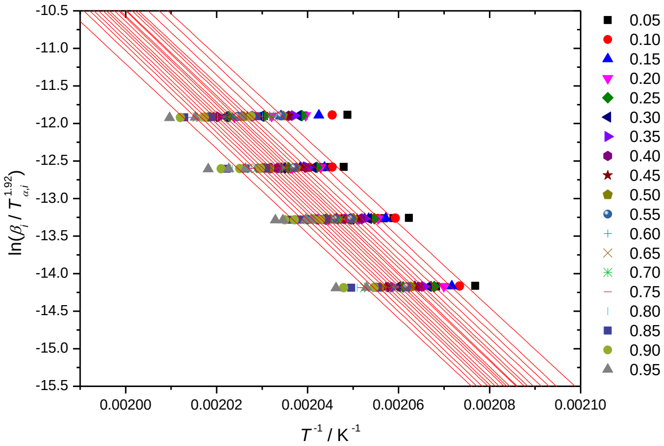

Fig. S3 The Starink plots for the extent of conversion (α) varying from 0.05 up to 0.95 (the sample **14-1**, the procedure A was applied to extract the heating branches from the $\chi_M T$ vs. T curves (see Fig S2)).

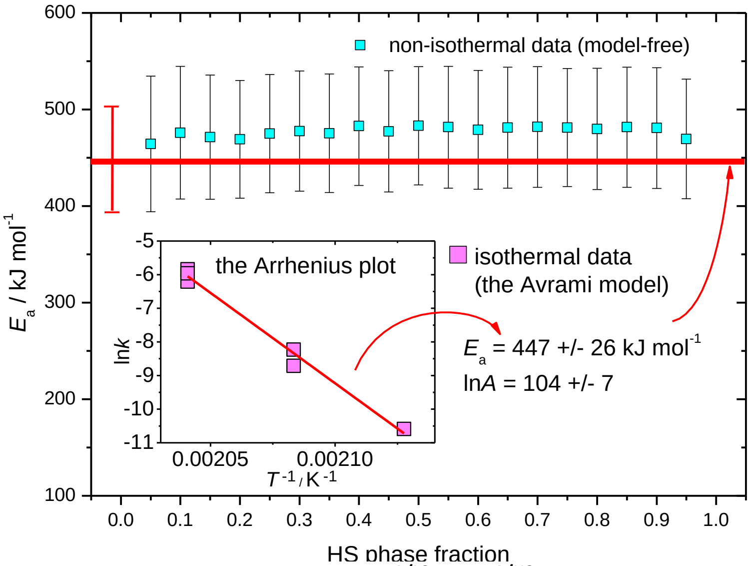

Fig. S4 Dependency of the activation energy of the $\mathbf{1}^{A/LS} \rightarrow \mathbf{1}^{A/HS}$ transition on the extent of conversion (sample **14-1**, the procedure A was applied to extract the heating branches from the $\chi_M T$ vs. T curves (see Fig S2)). The solid red line is the value obtained by the model-fitting method (the Avrami equation) from isothermal data. Inset: the Arrhenius plot of isothermal data.

[1] The splines have been used to connect the experimental points for all of the samples when the procedure A was applied. The isoconversional values of the activation energies in Fig. 5 are the ones obtained using this way of presentation of the normalized heating branches of the spin crossover curves. In some cases we also have tested fitting the normalized heating branches to the Avrami-type equation (see samples **14-1** and **5-1**), but obtained essentially identical estimates of the activation energy.

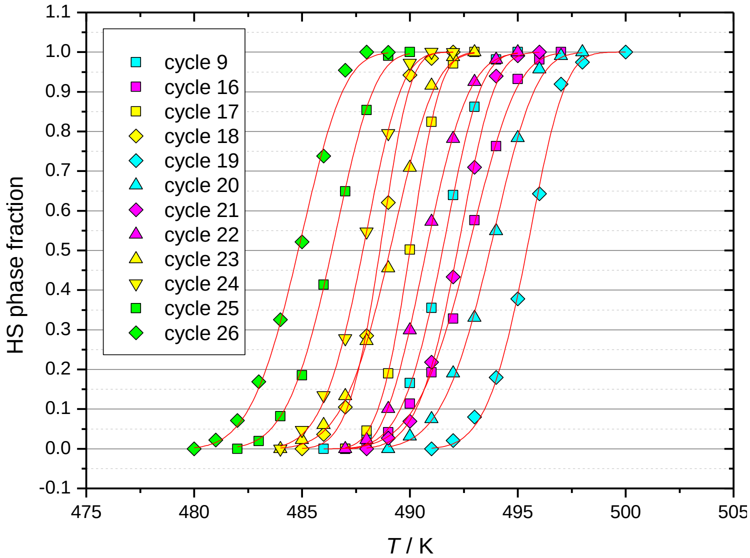

Fig. S5 The normalized heating branches of the $\chi_M T$ vs. T curves for the sample **14-1** (the procedure A was applied to extract the heating branches from the $\chi_M T$ vs. T curves). The solid lines are theoretical curves obtained by fitting to the Avrami-type equation, $\alpha = 1 - \exp(-(k(T - T_0))^n)$.

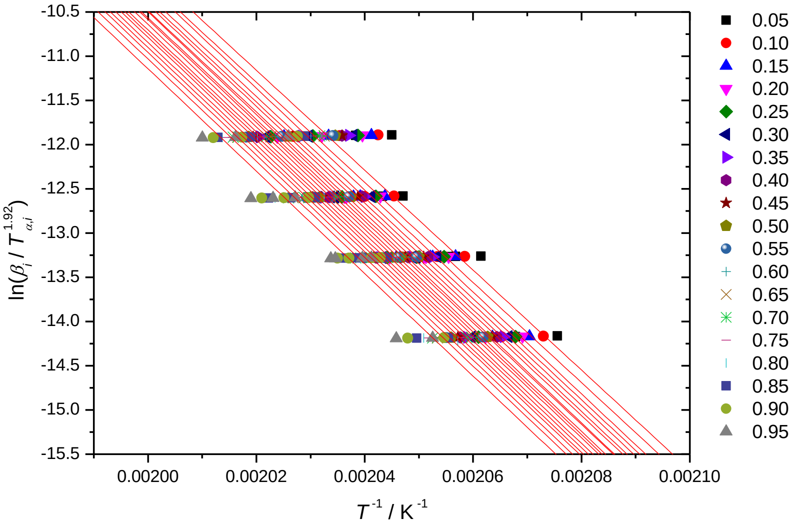

Fig. S6 The Starink plots for the extent of conversion (α) varying from 0.05 up to 0.95 (the sample **14-1**, the procedure A was applied to extract the heating branches from the $\chi_M T$ vs. T curves (see Fig S5)).

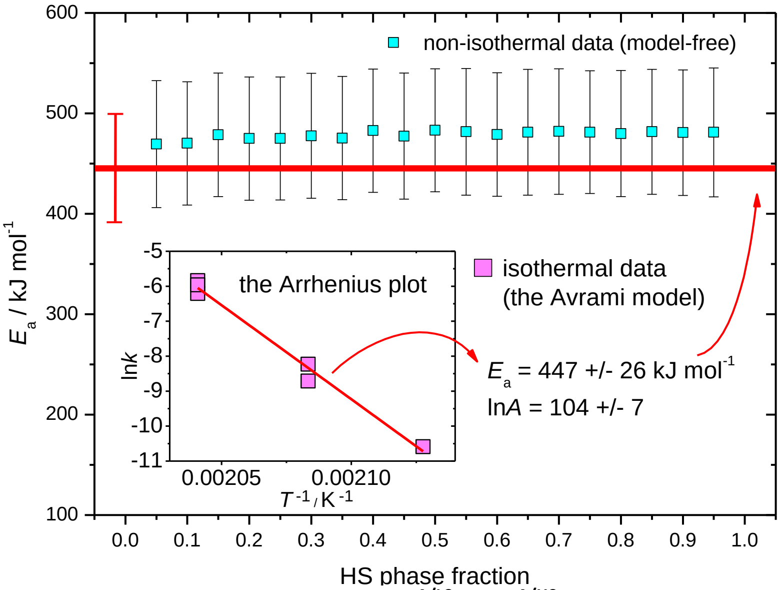

Fig. S7 Dependency of the activation energy of the $\mathbf{1}^{A/LS} \rightarrow \mathbf{1}^{A/HS}$ transition on the extent of conversion (sample **14-1**, the procedure A was applied to extract the heating branches from the $\chi_M T$ vs. T curves (see Fig S5)). The solid red line is the value obtained by the model-fitting method (the Avrami equation) from isothermal data. Inset: the Arrhenius plot of isothermal data.

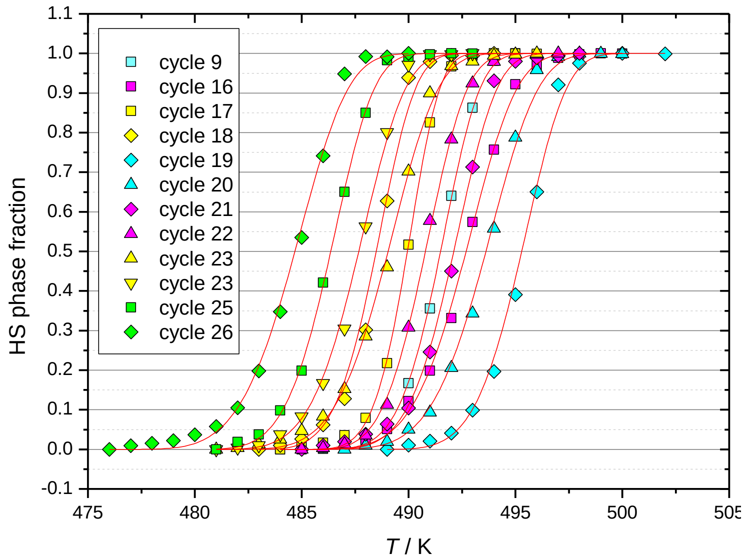

Fig. S8 The normalized heating branches of the $\chi_M T$ vs. T curves for the sample **14-1** (the procedure B was applied to extract the heating branches from the $\chi_M T$ vs. T curves). The solid lines are theoretical curves obtained by fitting to the Avrami-type equation, $\alpha = 1 - \exp(-(k(T - T_0))^n)$.

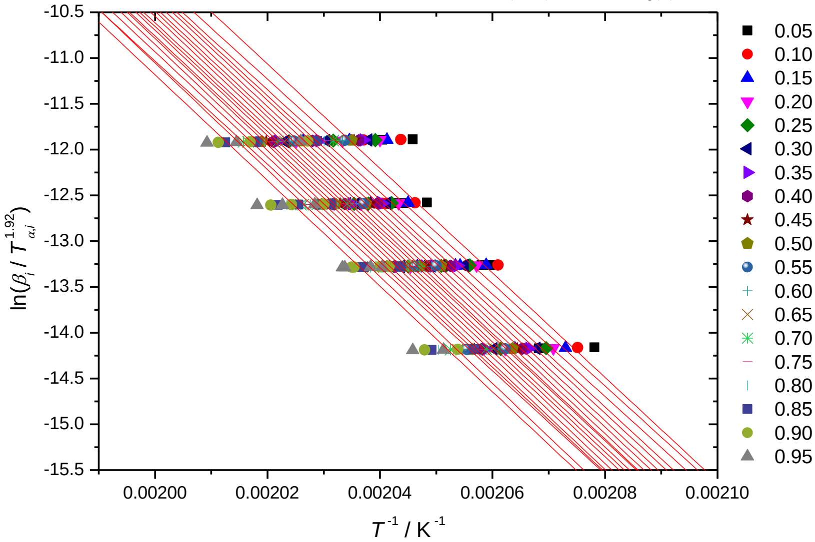

Fig. S9 The Starink plots for the extent of conversion (α) varying from 0.05 up to 0.95 (the sample **14-1**, the procedure B was applied to extract the heating branches from the $\chi_M T$ vs. T curves (see Fig S8)).

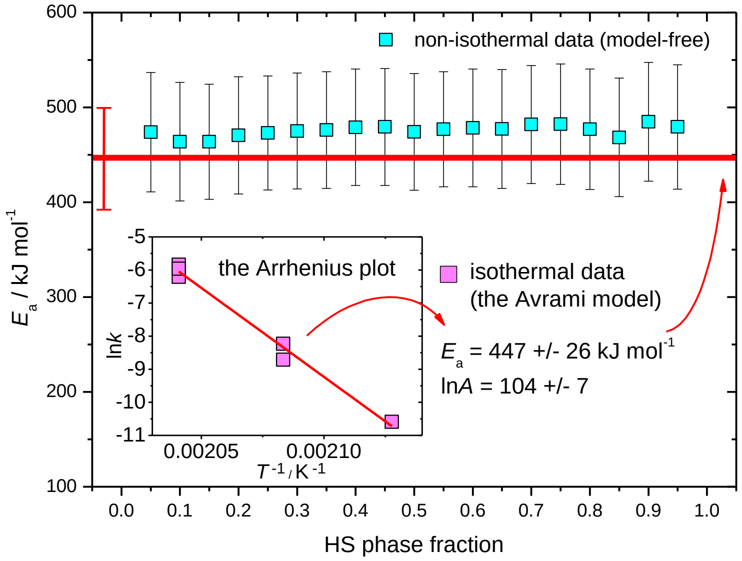

Fig. S10 Dependency of the activation energy of the $1^{A/LS} \rightarrow 1^{A/HS}$ transition on the extent of conversion (sample **14-1**, the procedure B was applied to extract the heating branches from the $\chi_M T$ vs. T curves (see Fig S8)). The solid red line is the value obtained by the model-fitting method (the Avrami equation) from isothermal data. Inset: the Arrhenius plot of isothermal data.

Table S1. Sample **14-1**: Information about thermal cycling, temperatures $T_c\uparrow$ and $T_c\downarrow$ (K), hysteresis loop width ΔT (K) and kinetic parameters for the LS $\rightarrow$ HS and the HS $\rightarrow$ LS transitions (the JMAK model and biexponential approximation). The spin transition temperatures $T_c\uparrow$ and $T_c\downarrow$ were determined in "dynamic" experiments by the maximum value of d($\chi_M T$)/dT; the temperatures at which kinetic measurements have been done are marked by "kin". The hysteresis loop widths are given only for the cycles when both heating and cooling were done in the non-isothermal mode.

sample	cycle	day	$T\uparrow$	n	k / s^{-1}	$T\downarrow$	τ_1 / s	τ_2 / s	ΔT
14	**1**	1st	**ca. 390**			**370 kin**			
	2	1st	**425**			**372**			**53**
	3	1st	**402**			**375**			**27**
	4	1st	**407**			**375**			**32**
	5	134th	**401**			**374**			**27**
	6	134th	**405**			**375**			**30**
14-1	**7**	179th	**490 kin**	1.85	1.26×10^{-4}	**358**			
	8	180th	**490 kin**	2.33	2.91×10^{-3}	**360 kin**	7.46×10^{1}	8.89×10^{2}	
	9	180th	**492**			**361**			**131**
	10	187th	**490 kin**	3.20	2.02×10^{-3}	**360 kin**	1.23×10^{2}	1.12×10^{3}	
	11	187th	**490 kin**	3.11	2.58×10^{-3}	**360 kin**	1.28×10^{2}	1.16×10^{3}	
	12	242nd	**480 kin**	3.72	1.64×10^{-4}				
	13	242nd	**480 kin**	4.17	2.67×10^{-4}	**362**			
	14	256th	**470 kin**	4.26	2.52×10^{-5}				
	15	263rd	**460 kin**						
	16	781st	**493**			**359**			**134**
	17	782nd	**490**			**361**			**129**
	18	795th	**489**			**361**			**128**
	19	876th	**496**			**360**			**136**
	20	876th	**494**			**360**			**134**
	21	885th	**492**			**359**			**133**
	22	886th	**491**			**360**			**131**
	23	901st	**490**			**360**			**130**
	24	902nd	**488**			**361**			**127**
	25	907th	**487**			**362**			**125**
	26	908th	**486**						

Sample 9

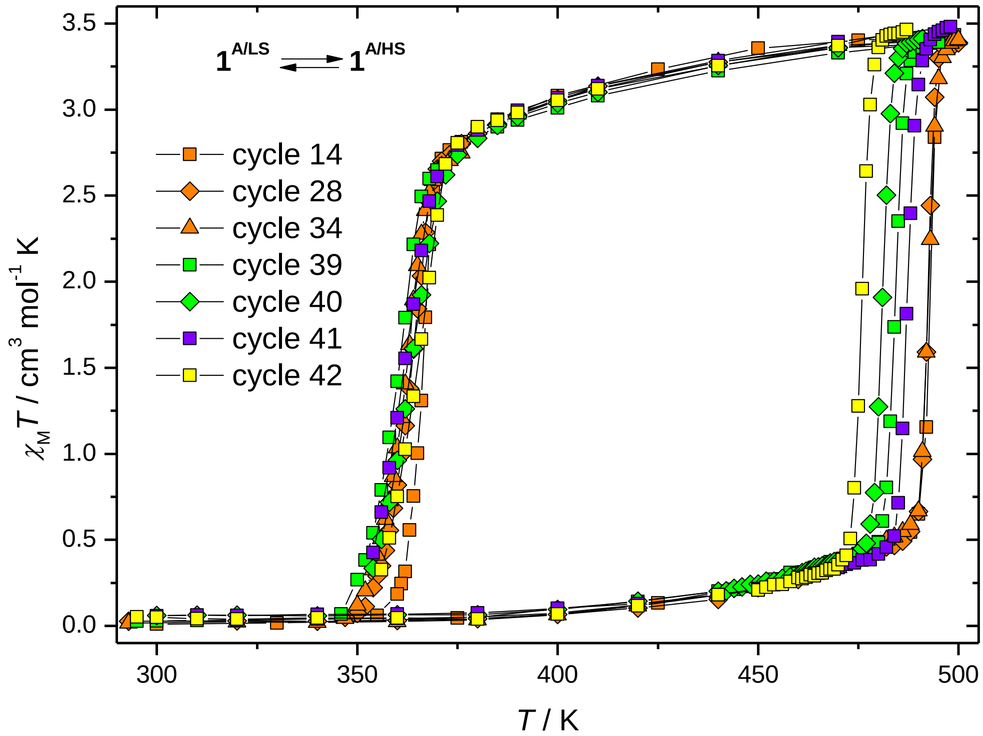

Fig. S11 Typical thermal cycles $\mathbf{1}^{A/LS} \leftrightarrow \mathbf{1}^{A/HS}$ for the sample **9**. Scan rates: 0.9 K min^{-1} (cycles 14, 28 and 34 orange), 0.5 K min^{-1} (cycle 41, blue), 0.1 K min^{-1} (cycles 39 and 40, green), 0.05 K min^{-1} (cycle 42, yellow).

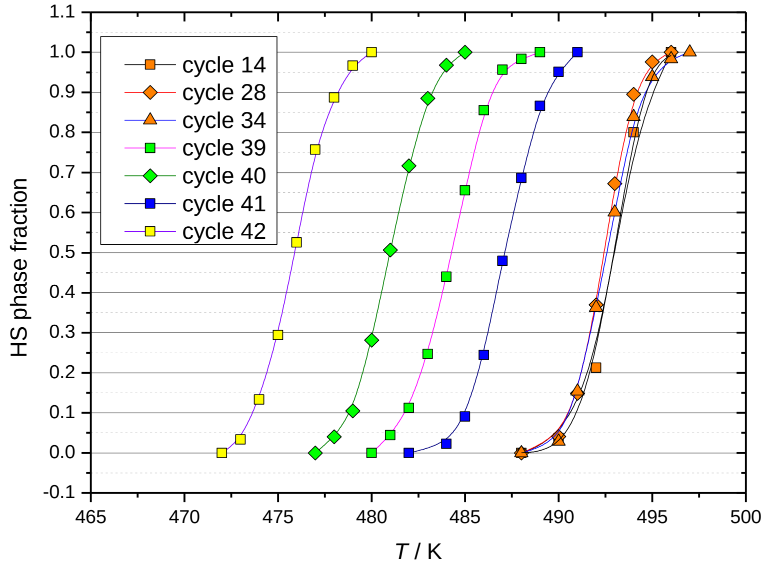

Fig. S12 The normalized heating branches of the $\chi_M T$ vs. T curves for the sample **9** (the procedure A was applied to extract the heating branches from the $\chi_M T$ vs. T curves). The solid lines are the B-splines.

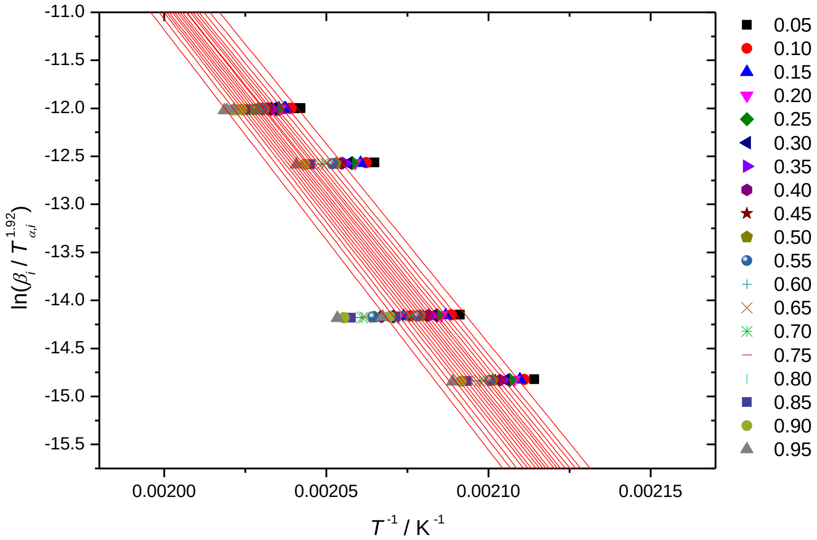

Fig. S13 The Starink plots for the extent of conversion (α) varying from 0.05 up to 0.95 (the sample **9**, the procedure A was applied to extract the heating branches from the $\chi_M T$ vs. T curves (see Fig S12)).

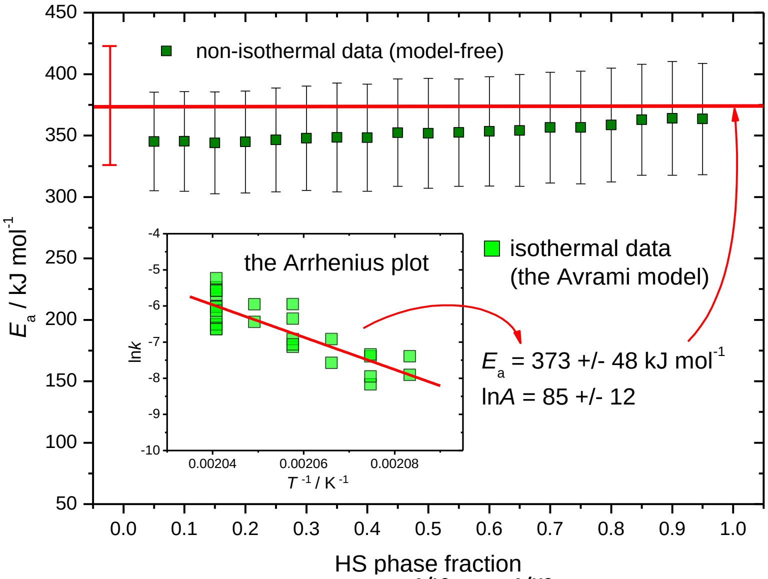

Fig. S14 Dependency of the activation energy of the $\mathbf{1}^{A/LS} \rightarrow \mathbf{1}^{A/HS}$ transition on the extent of conversion (sample **9**, the procedure A was applied to extract the heating branches from the $\chi_M T$ vs. T curves (see Fig S12)). The solid red line is the value obtained by the model-fitting method (the Avrami equation) from isothermal data. Inset: the Arrhenius plot of isothermal data.

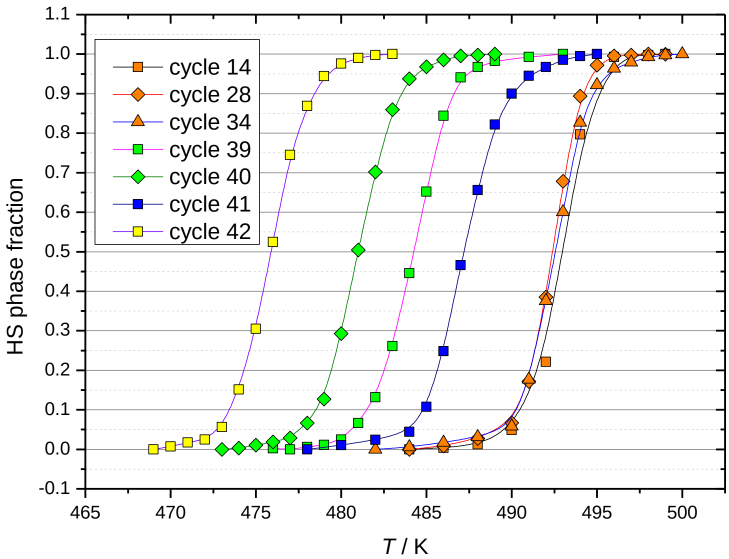

Fig. S15 The normalized heating branches of the $\chi_M T$ vs. T curves for the sample **9** (the procedure B was applied to extract the heating branches from the $\chi_M T$ vs. T curves). The solid lines are the B-splines.

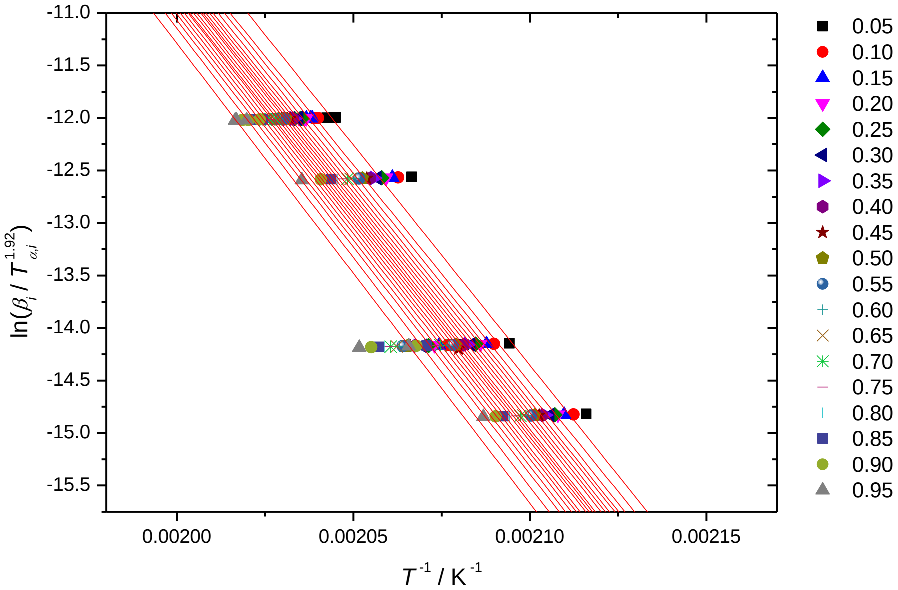

Fig. S16 The Starink plots for the extent of conversion (α) varying from 0.05 up to 0.95 (the sample **9**, the procedure B was applied to extract the heating branches from the $\chi_M T$ vs. T curves (see Fig S15)).

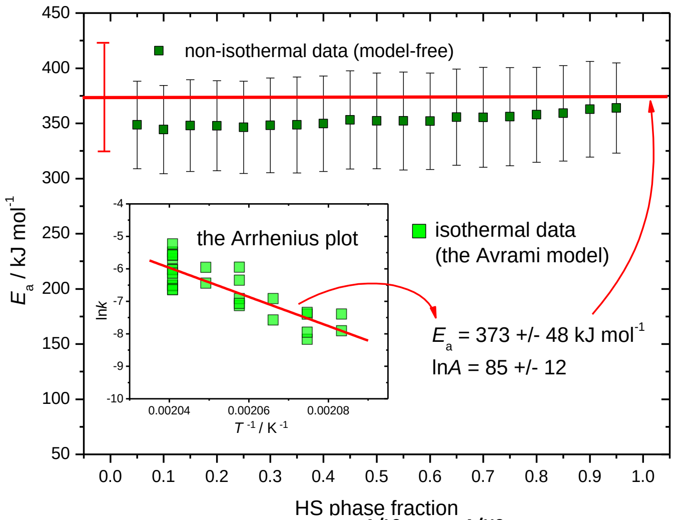

Fig. S17 Dependency of the activation energy of the $\mathbf{1}^{A/LS} \rightarrow \mathbf{1}^{A/HS}$ transition on the extent of conversion (sample **9**, the procedure B was applied to extract the heating branches from the $\chi_M T$ vs. T curves (see Fig S15)). The solid red line is the value obtained by the model-fitting method (the Avrami equation) from isothermal data. Inset: the Arrhenius plot of isothermal data.

Table S2. Sample **9**: Information about thermal cycling, temperatures $T_c\uparrow$ and $T_c\downarrow$ (K), hysteresis loop width ΔT (K) and kinetic parameters for the LS $\rightarrow$ HS (the JMAK model) and the HS $\rightarrow$ LS transitions (biexponential approximation). The spin transition temperatures $T_c\uparrow$ and $T_c\downarrow$ were determined in "dynamic" experiments by the maximum value of d($\chi_M T$)/dT; the temperatures at which kinetic measurements have been done are marked by "kin". The hysteresis loop widths are given only for the cycles when both heating and cooling were done in the non-isothermal mode.

sample	cycle	day	$T\uparrow$	n	k / s^{-1}	$T\downarrow$	τ_1	τ_2	ΔT
5	**1**	1st	**ca. 450**			**350**			
	2	2nd	**494 kin**	2.20	5.63×10^{-4}	**365 kin**			
	3	2nd	**490 kin**	2.37	3.40×10^{-3}	**372**			
	4	8th	**492 kin**	3.16	1.03×10^{-3}	**370 kin**	5.61×10^{1}	1.47×10^{3}	
	5	9th	**492 kin**	3.30	9.40×10^{-4}	**367**			
	6	116th	**492 kin**	2.77	1.12×10^{-3}	**370 kin**	3.07×10^{1}	1.12×10^{3}	
	7	117th	**492 kin**	3.67	1.51×10^{-3}	**370 kin**	3.64×10^{1}	1.18×10^{3}	
	8	117th	**492 kin**	2.45	4.07×10^{-3}	**370 kin**	4.37×10^{1}	9.74×10^{2}	
	9	117th	**490 kin**	2.26	4.15×10^{-3}	**370 kin**	5.07×10^{1}	1.01×10^{3}	
	10	118th	**490 kin**	3.50	1.31×10^{-3}	**370 kin**	2.31×10^{2}	1.86×10^{3}	
	11	118th	**490 kin**	2.44	3.78×10^{-3}	**370 kin**	3.87×10^{1}	9.40×10^{2}	
	12	123rd	**490 kin**	3.98	1.47×10^{-3}	**370 kin**	9.43×10^{1}	1.46×10^{3}	
	13	123rd	**490 kin**	3.56	2.42×10^{-3}	**370 kin**	8.24×10^{1}	1.59×10^{3}	
	14	171st	**494**			**367**			**127**
	15	173rd	**490 kin**	3.63	1.50×10^{-3}	**370 kin**	6.53×10^{2}	5.54×10^{3}	
	16	173rd	**490 kin**	3.05	3.80×10^{-3}	**367 kin**	4.96×10^{1}	9.76×10^{2}	
	17	173rd	**490 kin**	2.91	5.35×10^{-3}	**368 kin**	2.89×10^{1}	9.38×10^{2}	
	18	174th	**490 kin**	3.51	1.85×10^{-3}	**368 kin**	1.67×10^{2}	2.19×10^{3}	
	19	174th	**490 kin**	3.28	2.42×10^{-3}	**368 kin**			
	20	175th	**486 kin**	3.52	8.00×10^{-4}	**366 kin**	3.21×10^{1}	1.32×10^{3}	
	21	175th	**486 kin**	3.14	9.91×10^{-4}	**366 kin**	7.03×10^{1}	1.95×10^{3}	
	22	203th	**490 kin**	3.00	1.30×10^{-3}	**370 kin**	1.21×10^{2}	3.23×10^{3}	
	23	203th	**490 kin**	2.40	2.18×10^{-3}	**370 kin**	3.26×10^{1}	1.87×10^{3}	
	24	208th	**482 kin**	3.71	2.83×10^{-4}	**366 kin**	5.65×10^{1}	1.61×10^{3}	
	25	208th	**482 kin**	2.75	6.14×10^{-4}	**366 kin**	3.02×10^{1}	1.26×10^{3}	
	26	211th	**488 kin**	1.80	1.60×10^{-3}	**366 kin**	4.78×10^{1}	1.60×10^{3}	
	27	211th	**488 kin**	1.75	2.60×10^{-3}	**366 kin**	3.38×10^{1}	2.24×10^{3}	
	28	327th	**493**			**364**			**129**
	29	373rd	**486 kin**	2.75	8.55×10^{-4}	**366 kin**	5.77×10^{1}	1.89×10^{3}	
	30	373rd	**486 kin**	1.80	1.75×10^{-3}	**366 kin**	3.79×10^{1}	1.63×10^{3}	
	31	373rd	**486 kin**	1.69	2.61×10^{-3}	**366 kin**			
	32	450th	**482 kin**	3.20	3.53×10^{-4}	**370 kin**	5.90×10^{1}	5.82×10^{3}	
	33	450th	**482 kin**	2.16	6.49×10^{-4}	**370 kin**	5.93×10^{1}	2.95×10^{3}	
	34	491st	**493**	2.75		**363**			**130**
	35	527th	**484 kin**	2.50	5.14×10^{-4}	**370 kin**	3.20×10^{1}	5.34×10^{3}	
	36	527th	**484 kin**	2.21	9.92×10^{-4}	**370 kin**			
	37	533rd	**480 kin**	2.77	3.68×10^{-4}	**370 kin**	4.70×10^{1}	2.39×10^{3}	
	38	533rd	**480 kin**	2.25	6.17×10^{-4}	**370 kin**	8.20×10^{1}	4.12×10^{3}	
	39	1217th	**484**			**362**			**122**
	40	1219th	**481**			**364**			**117**
	41	1225th	**487**			**362**			**125**
	42	1226th	**476**			**368**			**108**

Sample 5-1

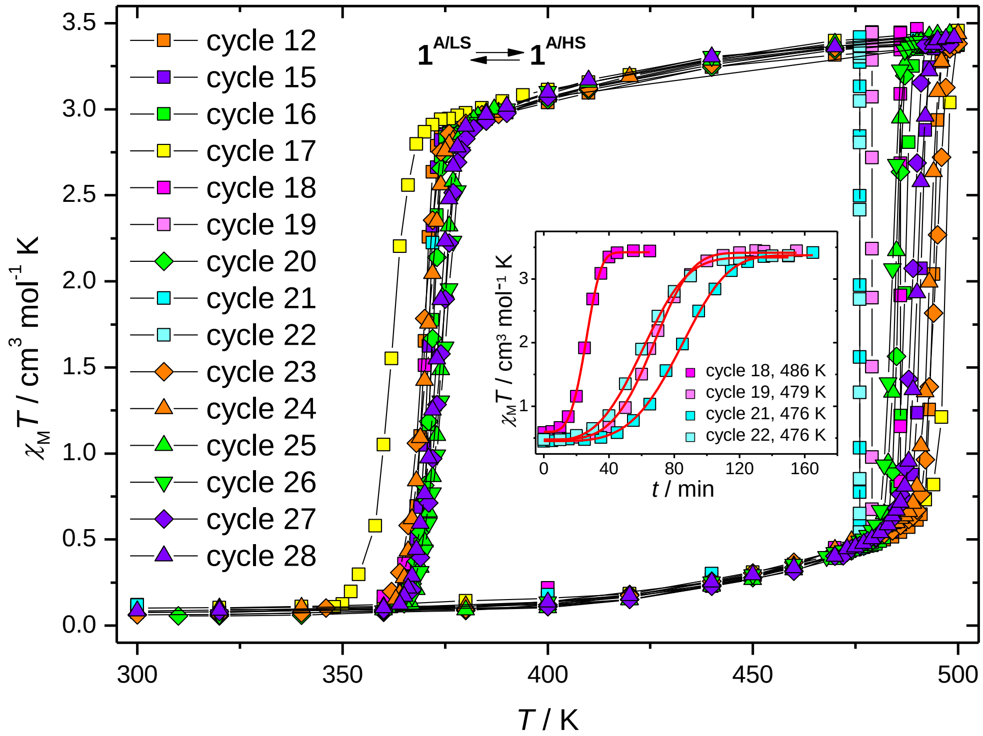

Fig. S18 Typical thermal cycles $\mathbf{1}^{A/LS} \leftrightarrow \mathbf{1}^{A/HS}$ for the sample **5-1**. Scan rates: 2 K min^{-1} (cycle 17, yellow), 1 K min^{-1} (cycles 23 and 24, orange), 0.9 K min^{-1} (cycle 12, orange), 0.5 K min^{-1} (cycles 27 and 28, violet), 0.4 K min^{-1} (cycle 15, violet), 0.25 K min^{-1} (cycles 16, 20, 25 and 26, green).

After *ca*. 1.5. years of ageing the sample **5-1** demonstrated wider hysteresis loop (cycle 17) than in preceding thermal cycles (compare with thermal cycles 12, 15 and 16) (Fig. S18). However, on further thermal cycling, the cooling branches of the $\chi_M T$ vs. T curves showed a good agreement with earlier magnetic cycles (Fig. S18).

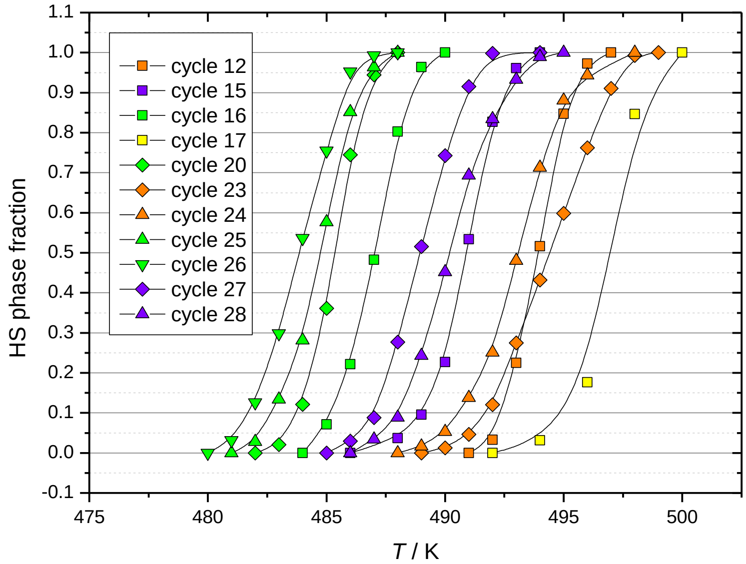

Fig. S19 The normalized heating branches of the $\chi_M T$ vs. T curves for the sample **5-1** (the procedure A was applied to extract the heating branches from the $\chi_M T$ vs. T curves). The solid lines are the B-splines.

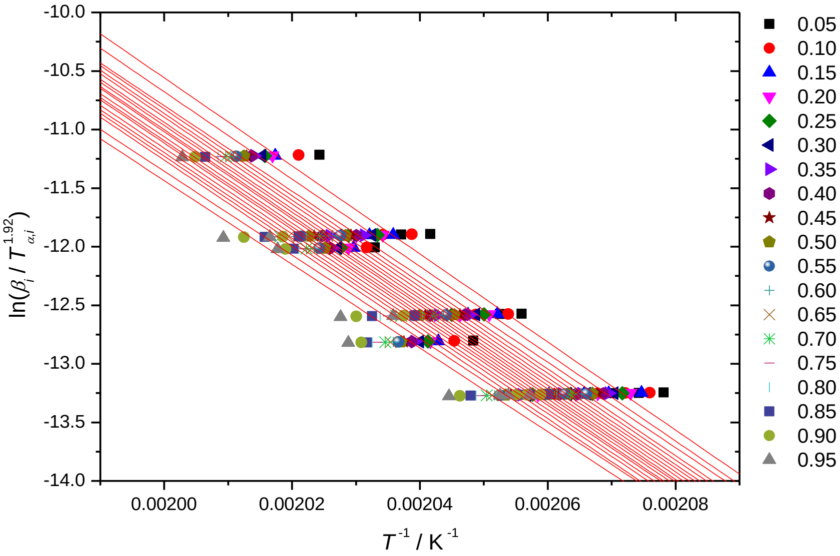

Fig. S20 The Starink plots for the extent of conversion (α) varying from 0.05 up to 0.95 (the sample **5-1**, the procedure A was applied to extract the heating branches from the $\chi_M T$ vs. T curves (see Fig S19)).

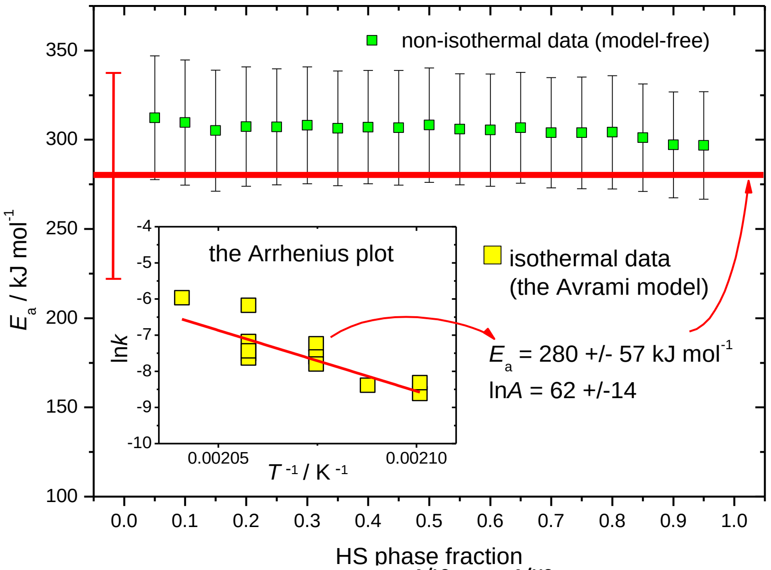

Fig. S21 Dependency of the activation energy of the $\mathbf{1}^{A/LS} \rightarrow \mathbf{1}^{A/HS}$ transition on the extent of conversion (sample **5-1**, the procedure A was applied to extract the heating branches from the $\chi_M T$ vs. T curves (see Fig S19)). The solid red line is the value obtained by the model-fitting method (the Avrami equation) from isothermal data. Inset: the Arrhenius plot of isothermal data.

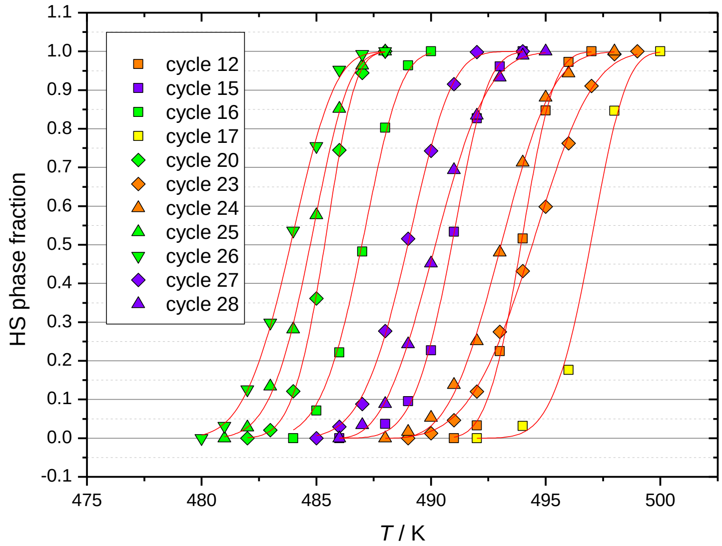

Fig. S22 The normalized heating branches of the $\chi_M T$ vs. T curves for the sample **5-1** (the procedure A was applied to extract the heating branches from the $\chi_M T$ vs. T curves). The solid lines are theoretical curves obtained by fitting to the Avrami-type equation, $\alpha = 1 - \exp(-(k(T - T_0))^n)$.

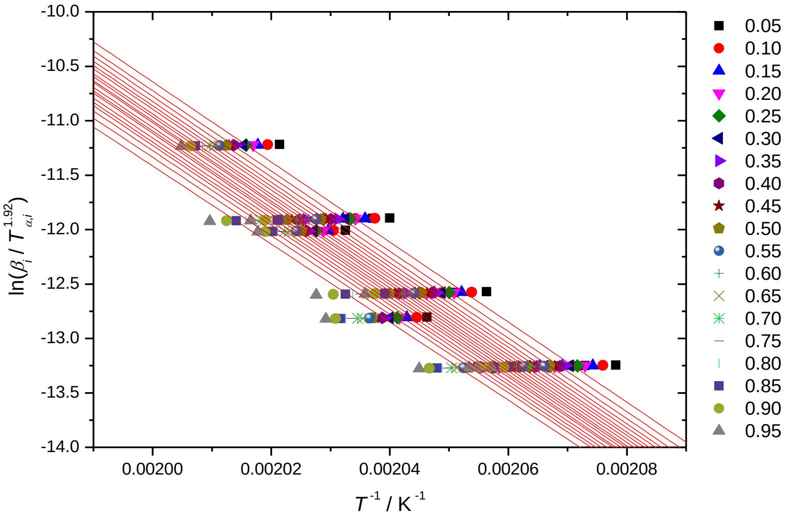

Fig. S23 The Starink plots for the extent of conversion (α) varying from 0.05 up to 0.95 (the sample **5-1**, the procedure A was applied to extract the heating branches from the $\chi_M T$ vs. T curves (see Fig S22)).

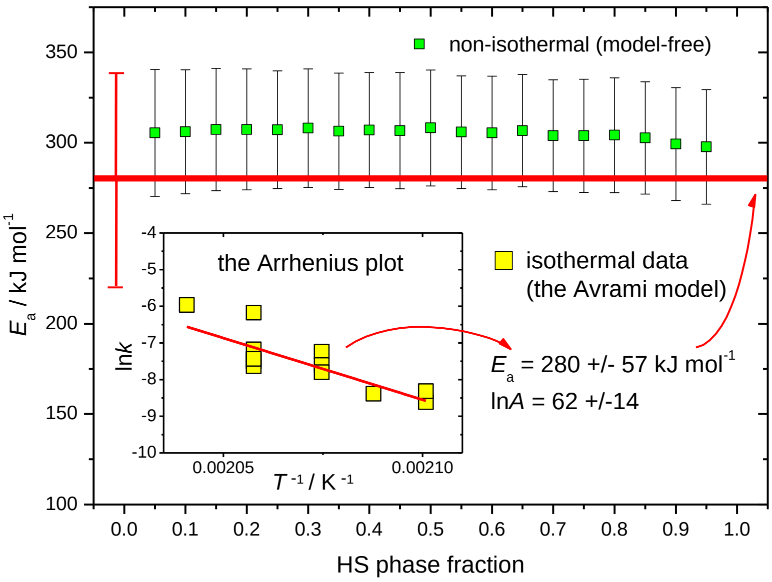

Fig. S24 Dependency of the activation energy of the $\mathbf{1}^{A/LS} \rightarrow \mathbf{1}^{A/HS}$ transition on the extent of conversion (sample **5-1**, the procedure A was applied to extract the heating branches from the $\chi_M T$ vs. T curves (see Fig S22)). The solid red line is the value obtained by the model-fitting method (the Avrami equation) from isothermal data. Inset: the Arrhenius plot of isothermal data.

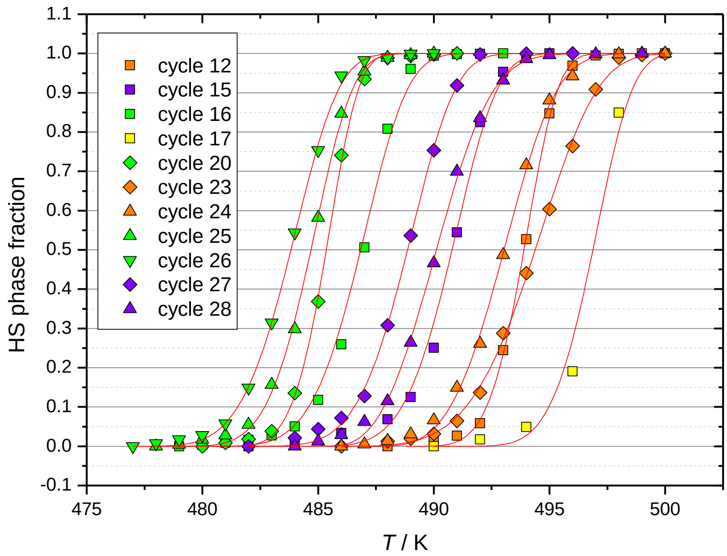

Fig. S25 The normalized heating branches of the $\chi_M T$ vs. T curves for the sample **5-1** (the procedure B was applied to extract the heating branches from the $\chi_M T$ vs. T curves). The solid lines are theoretical curves obtained by fitting to the Avrami-type equation, $\alpha = 1 - \exp(-(k(T - T_0))^n)$.

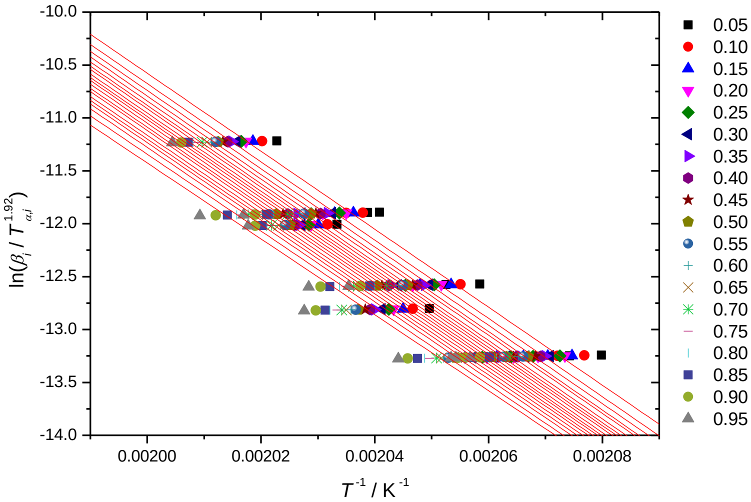

Fig. S26 The Starink plots for the extent of conversion (α) varying from 0.05 up to 0.95 (the sample **5-1**, the procedure B was applied to extract the heating branches from the $\chi_M T$ vs. T curves (see Fig S25)).

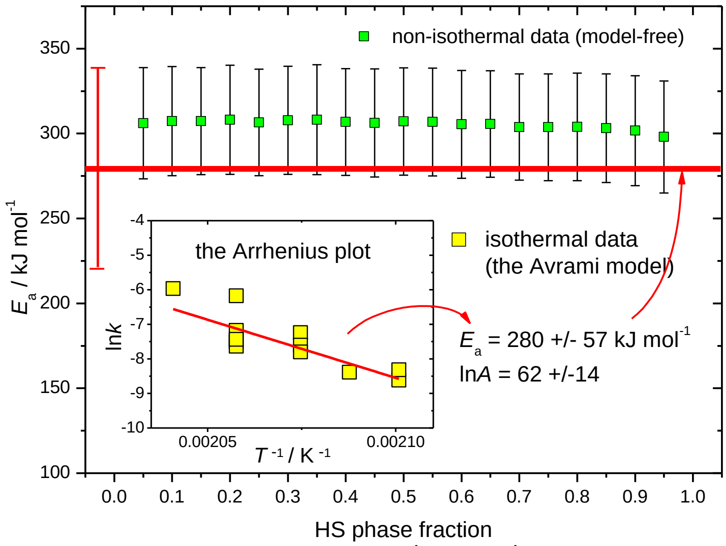

Fig. S27 Dependency of the activation energy of the $\mathbf{1}^{\mathbf{A/LS}} \rightarrow \mathbf{1}^{\mathbf{A/HS}}$ transition on the extent of conversion (sample **5-1**, the procedure B was applied to extract the heating branches from the $\chi_M T$ vs. T curves (see Fig S25)). The solid red line is the value obtained by the model-fitting method (the Avrami equation) from isothermal data. Inset: the Arrhenius plot of isothermal data.

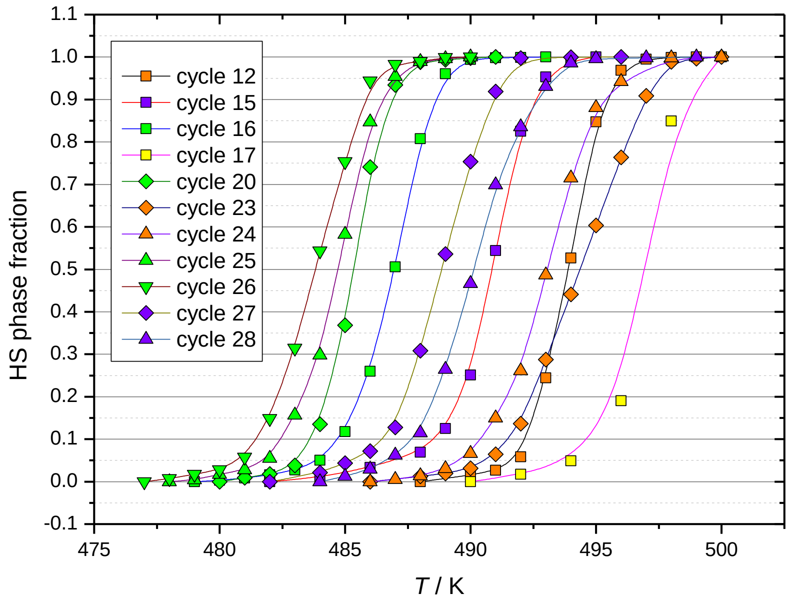

Fig. S28 The normalized heating branches of the $\chi_M T$ vs. T curves for the sample **5-1** (the procedure B was applied to extract the heating branches from the $\chi_M T$ vs. T curves). The solid lines are the B-splines.

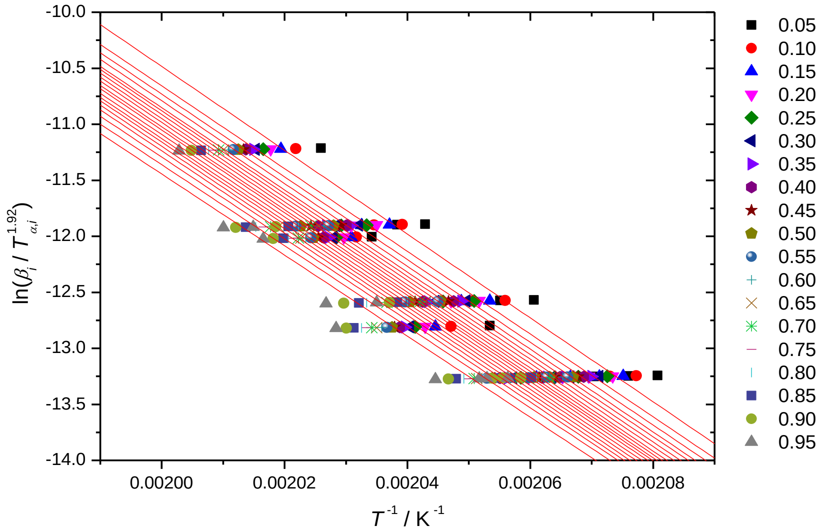

Fig. S29 The Starink plots for the extent of conversion (α) varying from 0.05 up to 0.95 (the sample **5-1**, the procedure B was applied to extract the heating branches from the $\chi_M T$ vs. T curves (see Fig S28)).

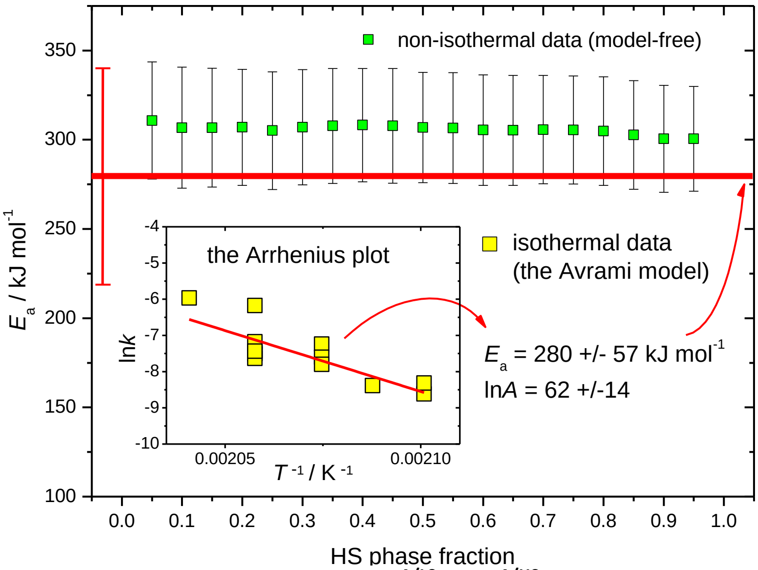

Fig. S30 Dependency of the activation energy of the $\mathbf{1}^{A/LS} \rightarrow \mathbf{1}^{A/HS}$ transition on the extent of conversion (sample **5-1**, the procedure B was applied to extract the heating branches from the $\chi_M T$ vs. T curves (see Fig. S28)). The solid red line is the value obtained by the model-fitting method (the Avrami equation) from isothermal data. Inset: the Arrhenius plot of isothermal data.

Table S3. Sample **5-1**: Information about thermal cycling, temperatures $T_c\uparrow$ and $T_c\downarrow$ (K), hysteresis loop width ΔT (K) and kinetic parameters for the LS → HS and the HS → LS transitions (the JMAK model and biexponential approximation). The spin transition temperatures $T_c\uparrow$ and $T_c\downarrow$ were determined in "dynamic" experiments by the maximum value of d($\chi_M T$)/dT; the temperatures at which kinetic measurements have been done are marked by "kin". The hysteresis loop widths are given only for the cycles when both heating and cooling were done in the non-isothermal mode.

sample	cycle	day	$T\uparrow$	n	k / s^{-1}	$T\downarrow$	τ_1 / s	τ_2 / s	ΔT
5	**1**	1st	**ca. 440**			**ca. 320**			
	2	18th	**ca. 320**			**ca. 320**			
5-1	**3**	23rd	**493**			**353**			**140**
	4	25th	**490 kin**	2.16	2.57×10^{-3}	**370 kin**		6.26×10^{3}	
	5	26th	**486 kin**	2.09	2.08×10^{-3}	**366 kin**	3.30×10^{2}	2.89×10^{3}	
	6	26th	**482 kin**	3.15	7.17×10^{-4}	**370**			
	7	28th	**482 kin**	3.51	4.98×10^{-4}	**370**			
	8	28th	**482 kin**	3.82	4.10×10^{-4}	**370**			
	9	131st	**486 kin**	3.77	5.48×10^{-4}	**373 kin**	5.19×10^{1}	4.88×10^{2}	
	10	131st	**486 kin**	3.92	7.64×10^{-4}	**373 kin**	9.35×10^{1}	1.07×10^{3}	
	11	131st	**486 kin**	3.99	5.49×10^{-4}	**373 kin**			
	12	168th	**494**			**370**			**124**
	13	309th	**486 kin**	4.00	5.84×10^{-4}	**373 kin**	1.96×10^{2}	1.50×10^{3}	
	14	309th	**486 kin**	3.65	4.84×10^{-4}	**373 kin**	2.39×10^{2}	1.67×10^{3}	
	15	388th	**491**			**371**			**120**
	16	393rd	**487**			**372**			**115**
	17	905th	**497**			**361**			**136**
	18	906th	**486 kin**	3.99	5.90×10^{-4}				
	19	906th	**479 kin**	4.05	2.28×10^{-4}				
	20	921st	**485**			**373**			**112**
	21	997th	**476 kin**	4.10	1.82×10^{-4}				
	22	997th	**476 kin**	3.26	2.45×10^{-4}				
	23	1024th	**495**			**370**			**125**
	24	1024th	**493**			**370**			**123**
	25	1031st	**485**			**375**			**110**
	26	1032nd	**484**			**375**			**109**
	27	1038th	**489**			**375**			**114**
	28	1039th	**490**			**374**			**116**

Sample 7

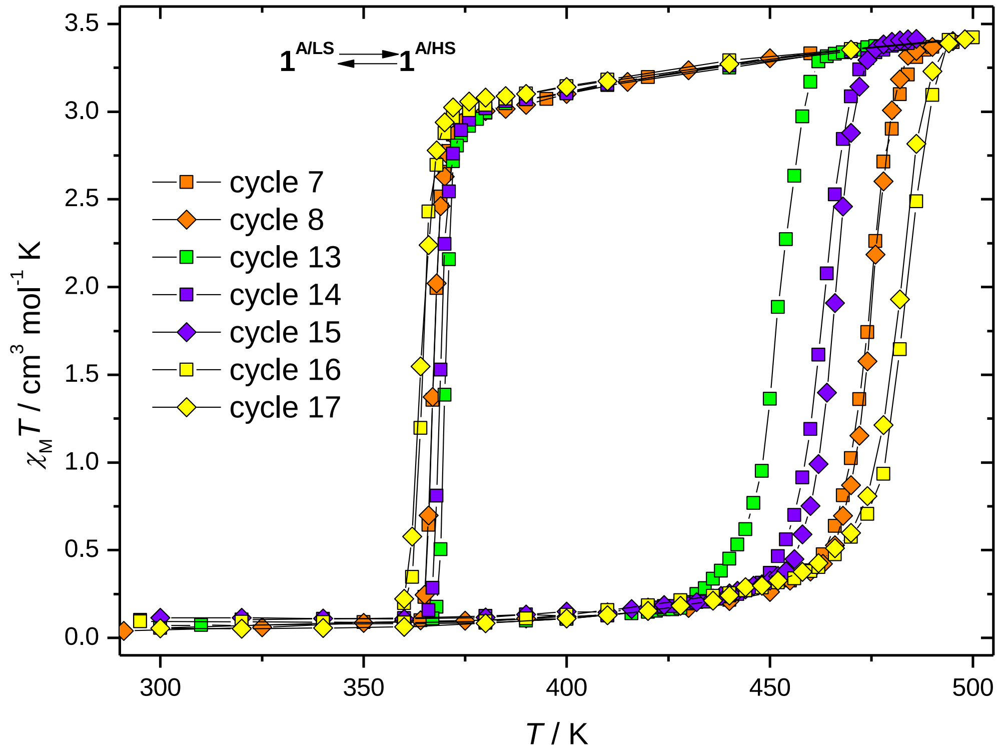

Fig. S31 Typical thermal cycles $\mathbf{1}^{A/LS} \leftrightarrow \mathbf{1}^{A/HS}$ for the sample **7**. Scan rates: 2 K min^{-1} (cycles 16 and 17, yellow), 0.9 K min^{-1} (cycles 7 and 8, orange), 0.5 K min^{-1} (cycles 14 and 15, blue), 0.25 K min^{-1} (cycle 13, green).

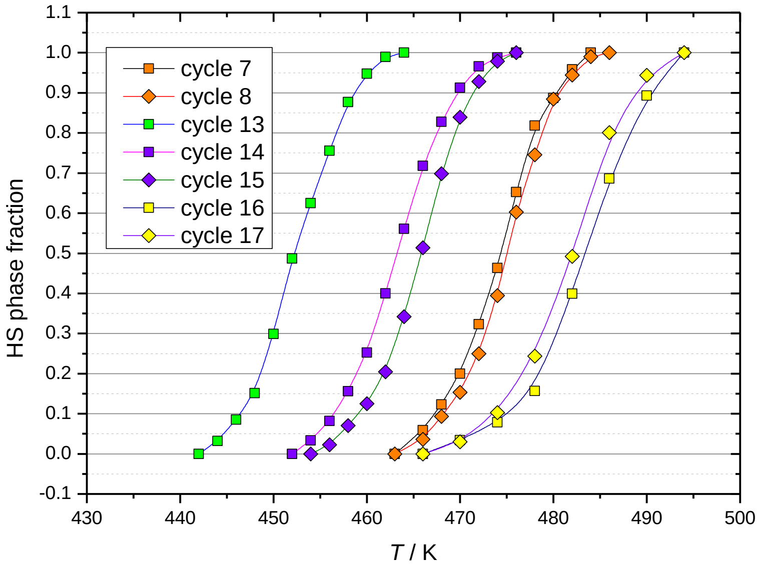

Fig. S32 The normalized heating branches of the $\chi_M T$ vs. T curves for the sample **7** (the procedure A was applied to extract the heating branches from the $\chi_M T$ vs. T curves). The solid lines are the B-splines.

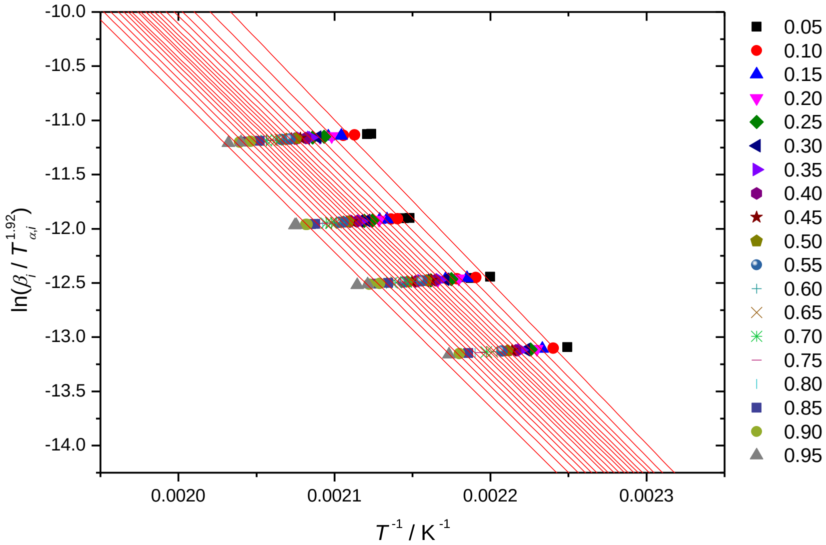

Fig. S33 The Starink plots for the extent of conversion (α) varying from 0.05 up to 0.95 (the sample **7**, the procedure A was applied to extract the heating branches from the $\chi_M T$ vs. T curves (see Fig S32)).

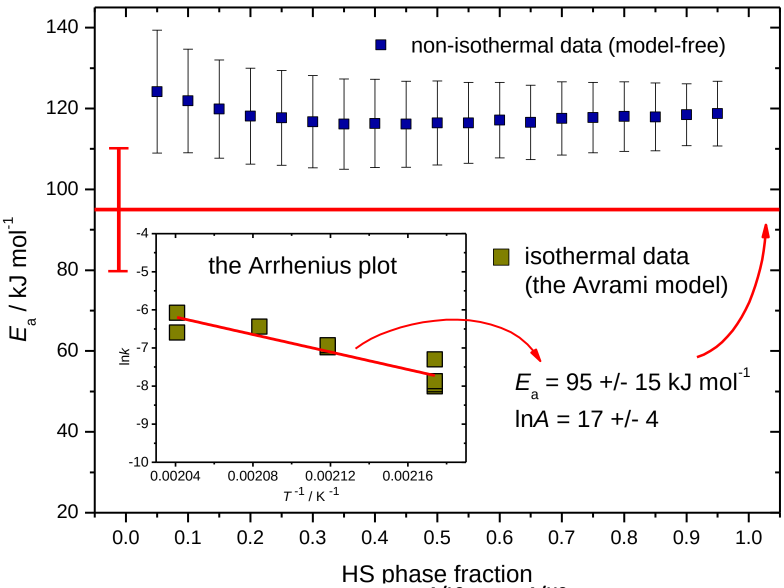

Fig. S34 Dependency of the activation energy of the $\mathbf{1}^{A/LS} \rightarrow \mathbf{1}^{A/HS}$ transition on the extent of conversion (sample **7**, the procedure A was applied to extract the heating branches from the $\chi_M T$ vs. T curves (see Fig S32)). The solid red line is the value obtained by the model-fitting method (the Avrami equation) from isothermal data. Inset: the Arrhenius plot of isothermal data.

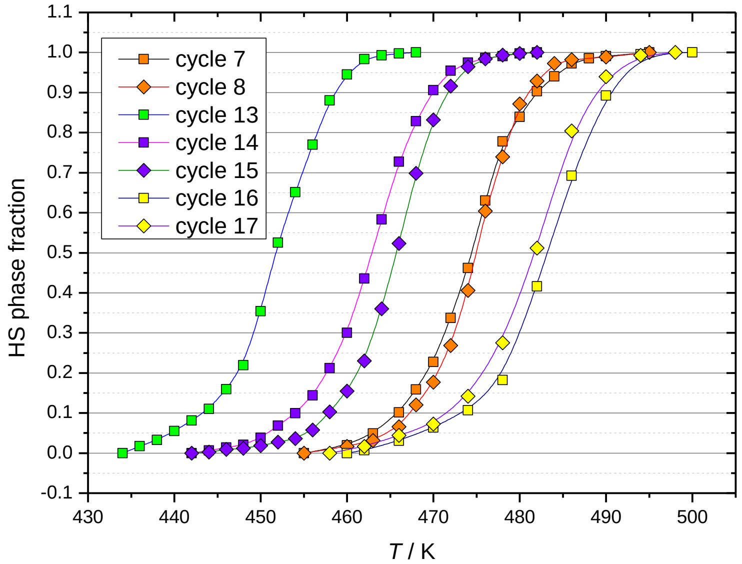

Fig. S35 The normalized heating branches of the $\chi_M T$ vs. T curves for the sample **7** (the procedure B was applied to extract the heating branches from the $\chi_M T$ vs. T curves). The solid lines are the B-splines.

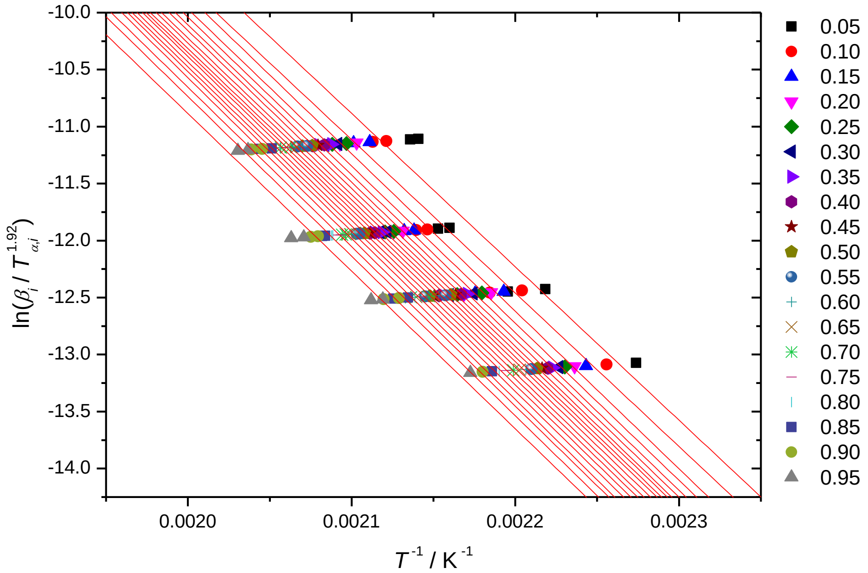

Fig. S36 The Starink plots for the extent of conversion (α) varying from 0.05 up to 0.95 (the sample **7**, the procedure B was applied to extract the heating branches from the $\chi_M T$ vs. T curves (see Fig S35)).

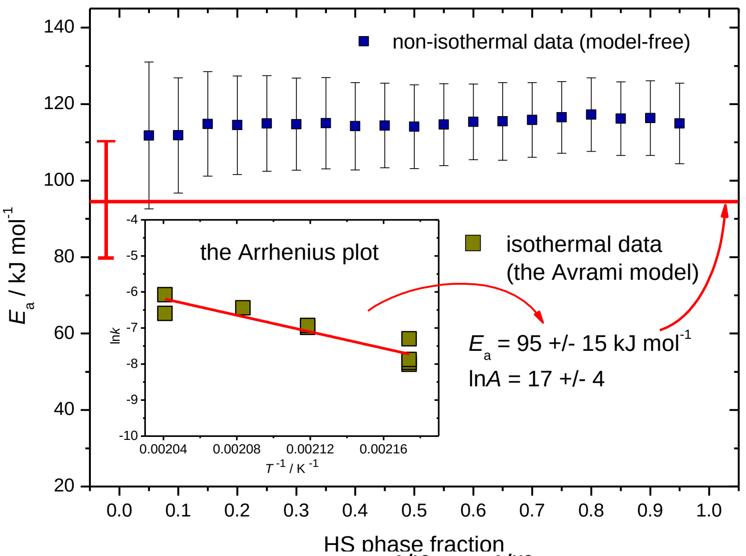

Fig. S37 Dependency of the activation energy of the $\mathbf{1}^{A/LS} \rightarrow \mathbf{1}^{A/HS}$ transition on the extent of conversion (sample **7**, the procedure B was applied to extract the heating branches from the $\chi_M T$ vs. T curves (see Fig S35)). The solid red line is the value obtained by the model-fitting method (the Avrami equation) from isothermal data. Inset: the Arrhenius plot of isothermal data.

Table S4. Sample **7**: Information about thermal cycling, temperatures $T_c\uparrow$ and $T_c\downarrow$ (K), hysteresis loop width ΔT (K) and kinetic parameters for the LS $\rightarrow$ HS and the HS $\rightarrow$ LS transitions (the JMAK model). The spin transition temperatures $T_c\uparrow$ and $T_c\downarrow$ were determined in "dynamic" experiments by the maximum value of $d(\chi_M T)/dT$; the temperatures at which kinetic measurements have been done are marked by "kin". The hysteresis loop widths are given only for the cycles when both heating and cooling were done in the non-isothermal mode.

sample	cycle	day	$T\uparrow$	n	k / s^{-1}	$T\downarrow$	n	k / s^{-1}	ΔT
7	**1**	1st	**-**			**360 kin**	1.56	9.45×10^{-4}	
	2	1st	**490 kin**	2.37	1.37×10^{-3}	**363 kin**	1.87	6.24×10^{-3}	
	3	1st	**490 kin**	1.87	2.30×10^{-3}	**365 kin**	2.82	3.65×10^{-3}	
	4	3rd	**480 kin**	2.09	1.59×10^{-3}	**370 kin**	2.58	1.42×10^{-3}	
	5	4th	**472 kin**	2.52	9.26×10^{-4}	**372 kin**	1.35	1.20×10^{-3}	
	6	4th	**472 kin**	2.32	9.79×10^{-4}	**370 kin**	1.56	3.18×10^{-3}	
	7	11th	**476**			**367**			**109**
	8	12th	**475**			**367**			**108**
	9	13th	**460 kin**	1.97	6.77×10^{-4}	**373 kin**	1.42	1.72×10^{-4}	
	10	13th	**460 kin**	2.14	3.33×10^{-4}	**371 kin**	2.16	4.07×10^{-4}	
	11	210th	**460 kin**	2.19	3.51×10^{-4}	**370 kin**	2.34	4.41×10^{-3}	
	12	210th	**460 kin**	2.27	3.81×10^{-4}	**370 kin**	2.50	3.59×10^{-3}	
	13	1058th	**450**			**370**			**80**
	14	1063rd	**464**			**369**			**95**
	15	1091st	**466**			**-**			
	16	1092nd	**482**			**364**			**118**
	17	1093rd	**482**			**364**			**118**

Sample 3

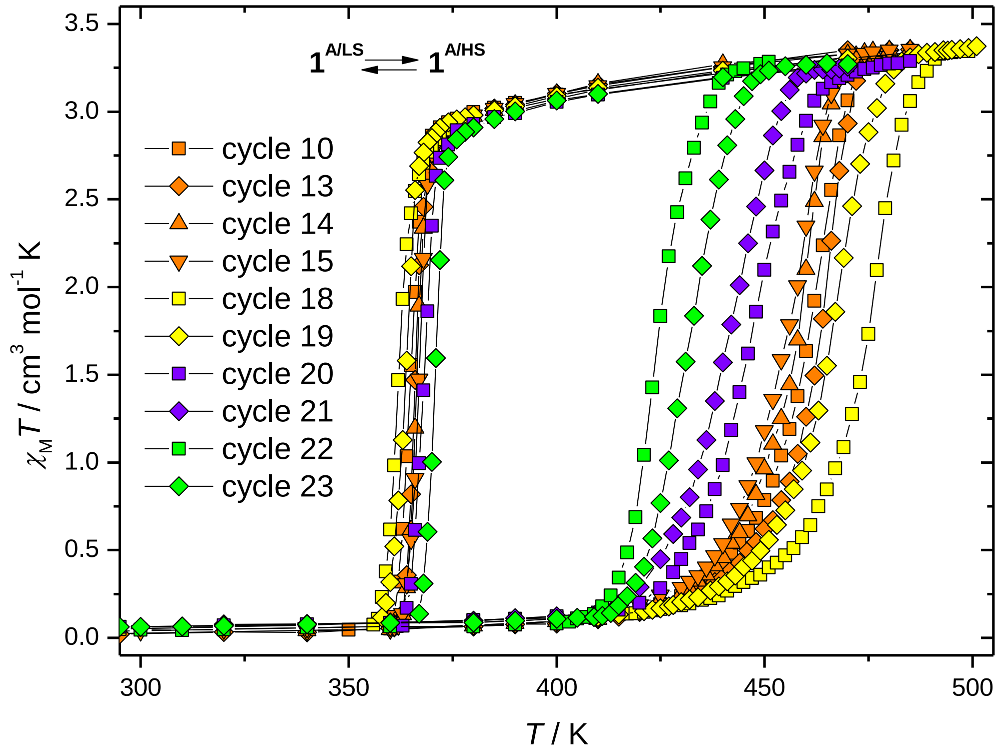

Fig. S38 Typical thermal cycles $\mathbf{1}^{A/LS} \leftrightarrow \mathbf{1}^{A/HS}$ for the sample **3**. Scan rates: 2 K min^{-1} (cycles 18 and 19, yellow), 0.9 K min^{-1} (cycles 10, 13, 14 and 15, orange), 0.5 K min^{-1} (cycles 21 and 22, blue), 0.25 K min^{-1} (cycles 22 and 23, green).

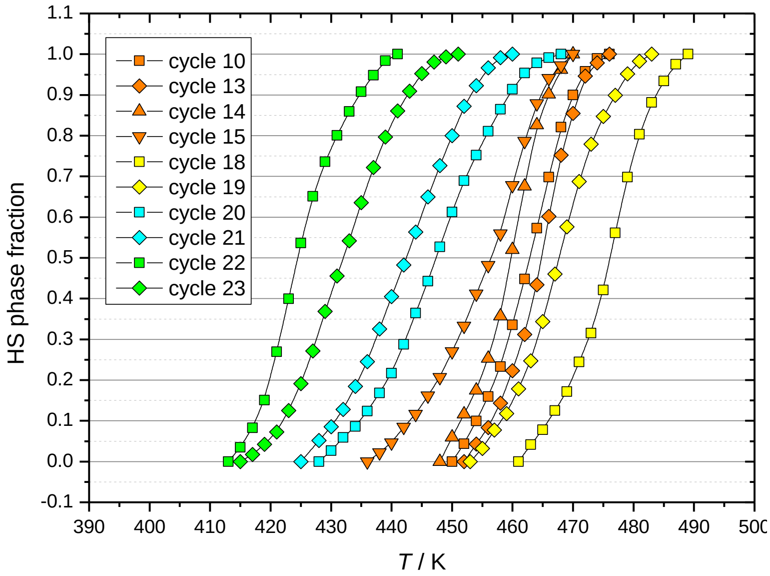

Fig. S39 The normalized heating branches of the $\chi_M T$ vs. T curves for the sample **3** (the procedure A was applied to extract the heating branches from the $\chi_M T$ vs. T curves). The solid lines are the B-splines.

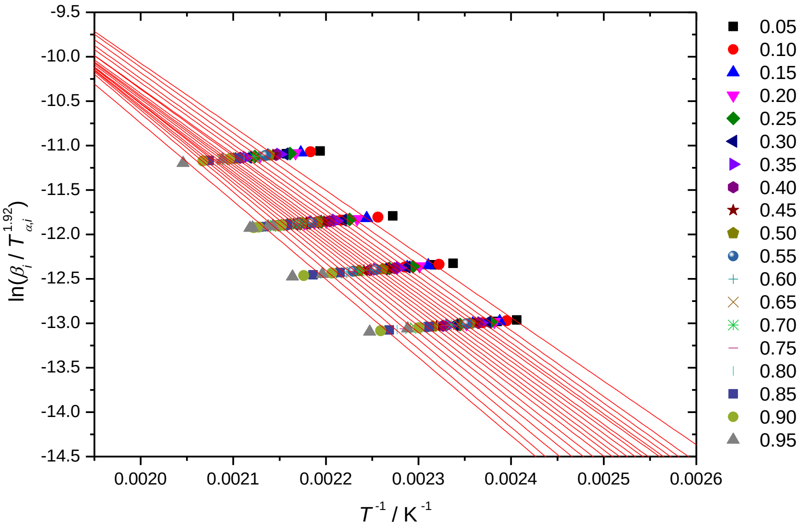

Fig. S40 The Starink plots for the extent of conversion (α) varying from 0.05 up to 0.95 (the sample **3**, the procedure A was applied to extract the heating branches from the $\chi_M T$ vs. T curves (see Fig S39)).

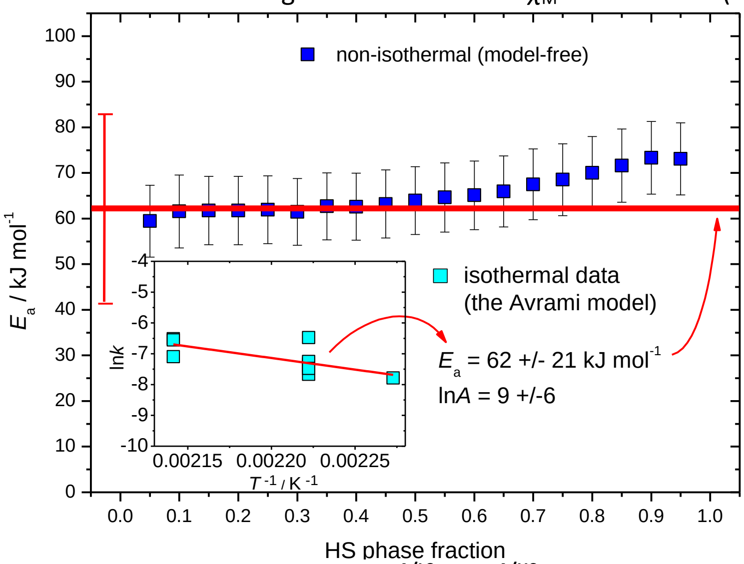

Fig. S41 Dependency of the activation energy of the $\mathbf{1}^{A/LS} \rightarrow \mathbf{1}^{A/HS}$ transition on the extent of conversion (sample **3**, the procedure A was applied to extract the heating branches from the $\chi_M T$ vs. T curves (see Fig S39)). The solid red line is the value obtained by the model-fitting method (the Avrami equation) from isothermal data. Inset: the Arrhenius plot of isothermal data.

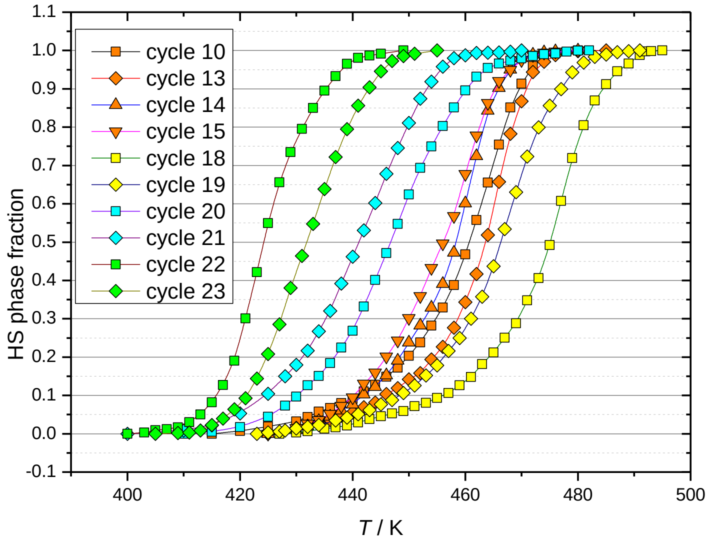

Fig. S42 The normalized heating branches of the $\chi_M T$ vs. T curves for the sample **3** (the procedure B was applied to extract the heating branches from the $\chi_M T$ vs. T curves). The solid lines are the B-splines.

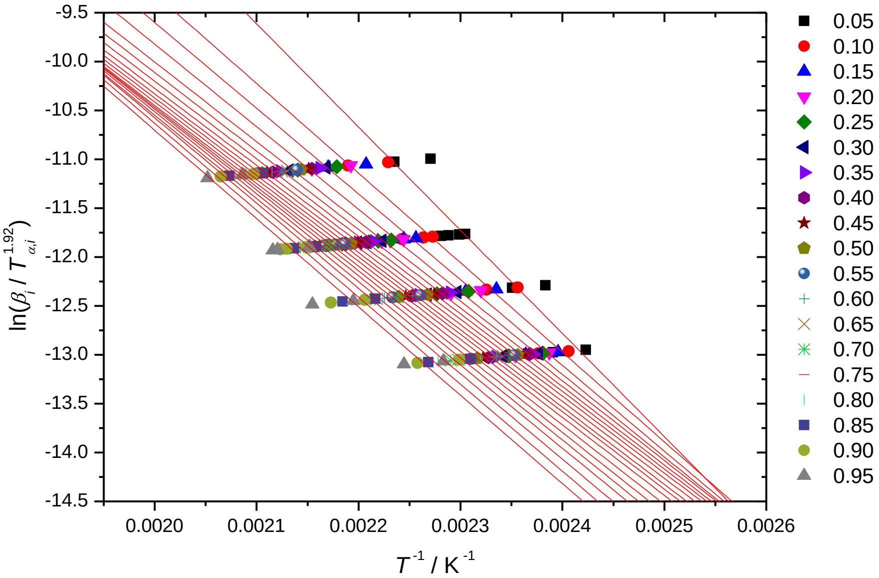

Fig. S43 The Starink plots for the extent of conversion (α) varying from 0.05 up to 0.95 (the sample **3**, the procedure B was applied to extract the heating branches from the $\chi_M T$ vs. T curves (see Fig S39)).

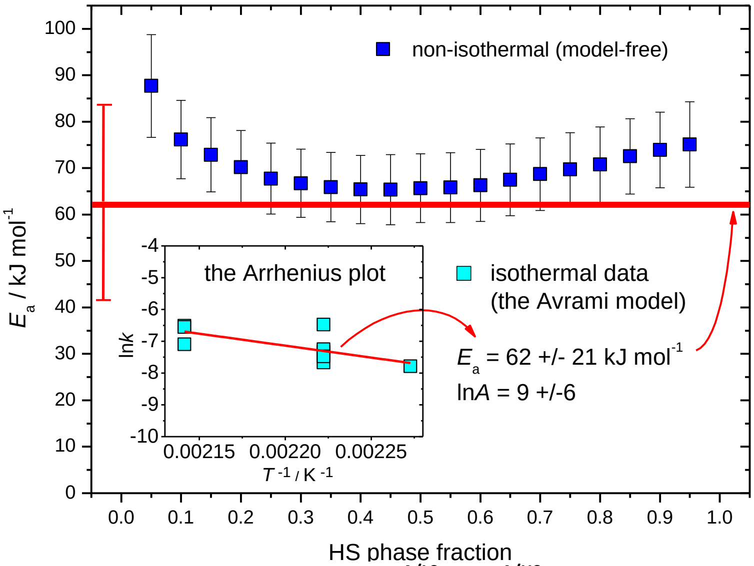

Fig. S44 Dependency of the activation energy of the $\mathbf{1}^{A/LS} \rightarrow \mathbf{1}^{A/HS}$ transition on the extent of conversion (sample **3**, the procedure B was applied to extract the heating branches from the $\chi_M T$ vs. T curves (see Fig S39)). The solid red line is the value obtained by the model-fitting method (the Avrami equation) from isothermal data. Inset: the Arrhenius plot of isothermal data.

Table S5. Sample **3**: Information about thermal cycling, temperatures T_c↑ and T_c↓ (K), hysteresis loop width ΔT (K) and kinetic parameters for the LS → HS and the HS → LS transitions (the JMAK model). The spin transition temperatures T_c↑ and T_c↓ were determined in "dynamic" experiments by the maximum value of $d(\chi_M T)/dT$; the temperatures at which kinetic measurements have been done are marked by "kin". The hysteresis loop widths are given only for the cycles when both heating and cooling were done in the non-isothermal mode.

sample	cycle	day	*T*↑	*n*	k / s^{-1}	*T*↓	*n*	k / s^{-1}	Δ*T*
3	**1**	1st	**ca. 385**			**360 kin**	4.40	7.37×10^{-4}	
	2	1st	**467 kin**	1.76	3.24×10^{-4}	**370 kin**	3.17	1.14×10^{-3}	
	3	1st	**467 kin**	1.72	8.30×10^{-4}	**370 kin**	3.52	1.00×10^{-3}	
	4	4th	**450 kin**	1.73	6.08×10^{-4}	**370 kin**	2.47	2.22×10^{-3}	
	5	4th	**450 kin**	2.18	4.67×10^{-4}	**370 kin**	2.99	1.40×10^{-3}	
	6	4th	**467 kin**	2.14	1.49×10^{-3}	**370 kin**	3.10	8.13×10^{-4}	
	7	9th	**450 kin**	1.77	6.60×10^{-4}	**370 kin**	2.47	1.67×10^{-3}	
	8	38th	**440 kin**	1.84	4.15×10^{-4}	**370 kin**	1.75	2.52×10^{-3}	
	9	38th	**467 kin**	1.99	1.43×10^{-3}	**370 kin**	2.68	1.11×10^{-3}	
	10	39th	**464**			**365**			**99**
	11	86th	**450 kin**	1.97	6.30×10^{-4}	**370 kin**	1.69	1.77×10^{-3}	
	12	86th	**450 kin**	2.15	1.54×10^{-3}	**370 kin**	2.00	1.64×10^{-3}	
	13	218th	**466**			**366**			**100**
	14	218th	**460**			**366**			**94**
	15	218th	**460**			**367**			**93**
	16	253rd	**450 kin**	2.06	7.10×10^{-4}	**370 kin**	1.46	1.17×10^{-3}	
	17	253rd	**450 kin**	2.08	5.66×10^{-4}	**370 kin**	2.00	2.83×10^{-3}	
	18	1088th	**477**			**362**			**115**
	19	1088th	**467**			**364**			**103**
	20	1089th	**448**			**369**			**79**
	21	1090th	**444**			**-**			
	22	1091th	**423**			**-**			
	23	1092th	**430**			**372**			**58**